




Influence of band structure on ballistic transport revealed by molecular nanoprobe

Andreas Christ ^{1,*} Patrick Härtl ¹ Patrick Kloster,¹ Matthias Bode ^{1,2} and Markus Leisegang ¹

¹Physikalisches Institut, Experimentelle Physik II, Universität Würzburg, Am Hubland, 97074 Würzburg, Germany

²Wilhelm Conrad Röntgen-Center for Complex Material Systems (RCCM), Universität Würzburg, Am Hubland, 97074 Würzburg, Germany



(Received 7 June 2022; revised 4 August 2022; accepted 26 August 2022; published 10 October 2022)

In this study we characterize the tautomerization of HPC on Cu(111) as a charge-carrier-induced reversible one-electron process. An analysis of the bias-dependent tautomerization rate finds an energy threshold that corresponds to the energy of the N-H stretching mode. By using the tautomerization of the molecule as a detector for charge carrier transport in the so-called molecular nanoprobe (MONA) technique, we provide evidence for an inhomogeneous coupling between the fourfold-symmetric molecule and sixfold-symmetric surface. We conclude the study by comparing the energy dependence of charge carrier transport on the Cu(111) to the Ag(111) surface. While the MONA technique is limited to the detection of hot-electron transport for Ag(111), our data reveal that the lower onset energy of the Cu surface state also allows for the detection of hot-hole transport. The influence of surface and bulk transport on the MONA technique is discussed.

DOI: [10.1103/PhysRevResearch.4.043016](https://doi.org/10.1103/PhysRevResearch.4.043016)

I. INTRODUCTION

In the past decades, the evolution of microelectronics followed Moore's law, which states that the number of transistors in integrated circuits doubles every two years. This trend mainly relied on the continued miniaturization of the transistor to a point, where the gate length is below 10 nm and single defects potentially compromise device functionality [1]. Although it is well known that step edges, defects, or the surface roughness significantly influence a material's transport properties [2–10], the investigation of electrical transport on atomic length scales, where the interaction of charge carriers with single discontinuities could be investigated, remains a challenging task.

The standard scientific tool to measure the electrical resistivity of solid-state materials is the four-point probe technique. Originally developed by Wenner as a means “to determine the resistivity of limited portions of the earth” more than 100 years ago [11], it was developed by generations of scientists to a versatile platform which is nowadays broadly used as an “interdisciplinary characterization tool in materials science, semiconductor industries, geology, physics, etc.” [12]. However, the four-point probe technique offers only limited access to atomic-scale charge transport properties. This limitation is caused by the finite radius of the probes, which is in the range between 10 to 20 nm under reasonably ideal circumstances. As a consequence, probe spacings below twice the radius, i.e., 20–40 nm, cannot be achieved [13,14].

To understand charge transport behavior on atomic length scales, novel measurement techniques need to be developed. One option is to abandon all but one tip and to use the only remaining tip of a conventional scanning tunneling microscope (STM) to locally inject electrical charge carriers, i.e., electrons or holes, into the sample surface. The high resolution of an STM enables the measurement of transport over distances of single nanometers. In addition, to achieve the goal of a transport measurement technique with atomic-scale spatial resolution, a sufficiently small charge detector needs to be identified. Based on earlier experiments performed by Liljeroth and co-workers [15], we recently proposed that the reversible switching of single molecules between multiple stable states may serve this role. Correspondingly, we termed this technique “molecular nanoprobe” (MONA).

Several detector molecules offering various molecular switching processes have been used so far. Based on earlier work by Liljeroth and co-workers [15], who observed the direct STM-induced tautomerization of naphthalocyanine molecules, Kügel and co-workers [16] analyzed the tautomerization process of phthalocyanine (Pc) molecules in more detail. Pc tautomerization is mediated by the N-H stretching mode which can be excited by inelastic electron scattering with a threshold energy $E_{\text{th}} \approx 408$ meV, i.e., “hot electrons” energetically far above the Fermi level. In contrast, the rotation of *cis*-2-buten on Pd(110) exhibits a much lower threshold energy of ≈ 30 mV only [17,18]. It has been shown by Ladenthin and co-workers [19], that this process can even be triggered by hot electrons injected into the substrate up to 100 nm away from the detector molecule. In the meantime, several studies that explore the influence of atom-by-atom-assembled nanostructures [20,21], substituents [22], or the impact of anisotropic surfaces [18] have been performed.

However, most of these MONA studies were restricted to the investigation of hot electron transport, whereas the transport of holes has not yet been investigated. The reason

*Corresponding author: andreas.christ@physik.uni-wuerzburg.de

Published by the American Physical Society under the terms of the [Creative Commons Attribution 4.0 International license](https://creativecommons.org/licenses/by/4.0/). Further distribution of this work must maintain attribution to the author(s) and the published article's title, journal citation, and DOI.

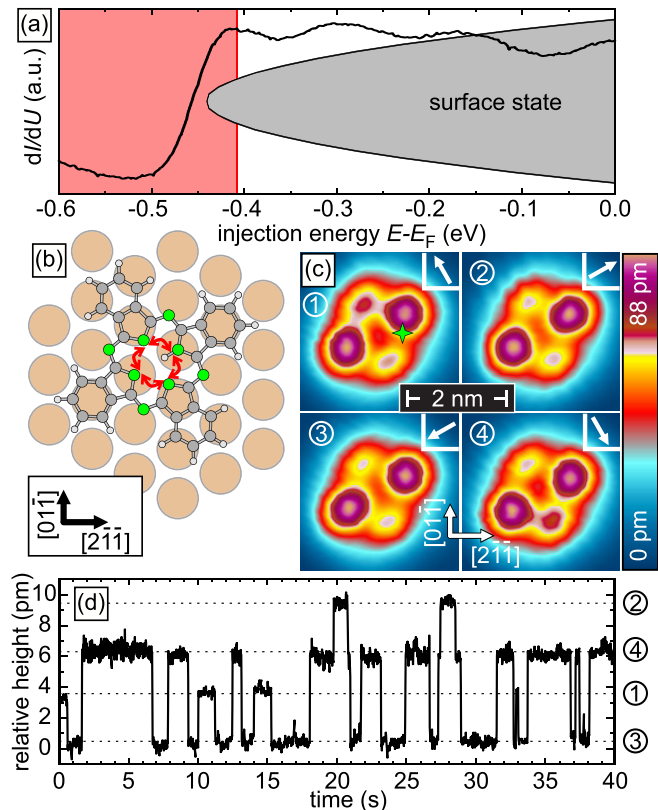


FIG. 1. (a) Tunneling spectrum of the Cu(111) surface (black line). As indicated by the gray parabola, the steplike increase of the dI/dU signal at $E - E_F = eU \approx 450$ meV represents the onset of the Cu(111) surface state. The threshold energy for HPC tautomerizations which amounts to $E_{th} = 408$ meV is exceeded in the red-shaded regime. (b) Schematic structure of HPC and the Cu(111) surface (carbon: gray; nitrogen: green; hydrogen: white). (c) Topographic scans of the four different tautomers of HPC on Cu(111) ($U = 50$ mV, $I = 50$ pA). White arrows indicate the binding position of the central hydrogen. (d) Telegraph noise measured with the tip positioned at the green cross in panel (c). The four distinct height levels are labeled with the corresponding tautomeric state.

becomes clear when looking at the electronic structure of the substrate most often used in these studies, i.e., Ag(111) [20–22]. Surface transport in Ag(111) is dominated by an s , p -derived, electron-like surface state with an onset energy $E_{on}^{Ag} \approx -63$ meV [23]. As a result, the N-H stretching mode of Pc molecules can readily be excited by hot electrons, whereas hot holes with sufficient energy are energetically located far below E_{on}^{Ag} , where no surface state is available any more.

To study tautomerization processes which are remotely excited by hot holes, we present a MONA investigation of phthalocyanine molecules on a Cu(111) substrate which offers a much lower surface state onset at around $E_{on}^{Cu} \approx -450$ meV, i.e., $|E_{on}^{Cu}| > E_{th}$; see Fig. 1(a). This lower surface state onset of Cu(111) allows us to measure hole and electron transport on the same substrate. Additionally, we investigate the transition from surface to bulk transport at negative energies with the MONA technique.

II. EXPERIMENTAL SETUP AND PROCEDURE

Sample preparation and analysis were proceeded in two separated chambers (base pressure $p \approx 1 \times 10^{-10}$ mbar). The Cu(111) single crystal was prepared by cycles of 30 min Ar^+ sputtering at an ion energy of 700 eV, followed by 20 min annealing at $T \approx 700$ K. Phthalocyanine molecules (H_2Pc ; Sigma-Aldrich) were deposited onto the clean Cu(111) surface at room temperature with a four-cell evaporator (Dodecon) from a filament-heated crucible. Data were measured with a low-temperature STM at a temperature $T \approx 4.5$ K operated in the constant-current mode.

After deposition, single molecules are randomly distributed across the surface. To exclude the influence of defects and surrounding molecules, lateral manipulation of H_2Pc molecules is necessary. Following the general recipes described in Ref. [24], the attractive interaction between molecule and tip at tunneling parameters $U = 20$ mV and $I = 5 \dots 50$ nA allows us to pull the investigated molecule to a defect-free area (20×20 nm²) and remove all other molecules in close vicinity. In the next step, one central proton can be removed by applying a bias voltage $U \geq 2.2$ V with the STM tip positioned directly above the molecule [25]. The resulting single HPC molecule is located in a defect-free adsorption site on the Cu(111) surface and separated by at least 10 nm from any other molecule.

III. RESULTS

A. On-top measurements

The schematic structure of a deprotonated phthalocyanine molecule (HPC) superimposed to the atomic lattice of a Cu(111) surface is shown in Fig. 1(b). Our data reveal that HPC molecules adsorb on Cu(111) similarly to Ag(111) [20] on bridge sites. HPC consists of four degenerated isoindol groups composed of carbon (gray), nitrogen (green), and hydrogen (white) atoms linked by nitrogen atoms. Due to the symmetry mismatch between the molecule (fourfold) and the surface (sixfold), however, the degeneracy between the arms is lifted upon adsorption on Cu(111). At imaging parameters of 50 mV and 50 pA, this manifests in different apparent heights of the isoindol groups—in the following described as arms—pointing along the closed-packed $[01\bar{1}]$ and the $[2\bar{1}\bar{1}]$ axes of the Cu(111) substrate, as displayed in the constant-current images shown in Fig. 1(c).

The degeneracy is further reduced by the only remaining central hydrogen atom which can bind to any of the four arms and thereby defines four different tautomers. In the STM topography images presented in panels 1 through 4 of Fig. 1(c), the four tautomers of HPC can be distinguished by subtle changes of the corresponding arm. For arms along the $[01\bar{1}]$ axis (panels 2 and 3) the presence of the H atom results in an elongation of the respective arm (see the Appendix), while the apparent height is slightly elevated if the H atom is bound to an arm oriented along the $[2\bar{1}\bar{1}]$ axis (1 and 4).

Switching between these tautomers can be triggered by injecting charge carriers above a certain threshold into the molecule [26]. With the tip positioned at the green cross in Fig. 1(c), these switches can simultaneously be induced

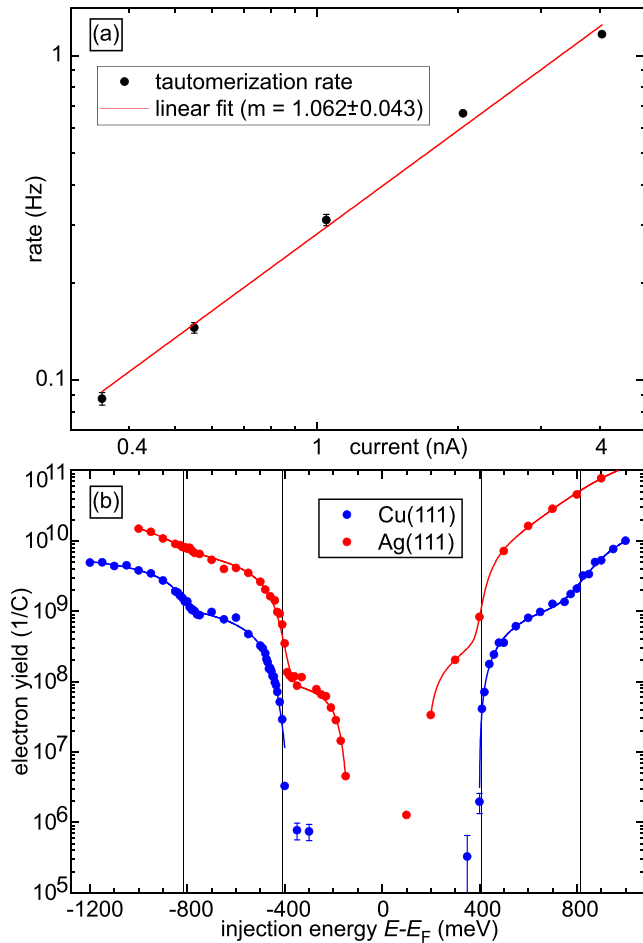


FIG. 2. (a) Current-dependent tautomerization rate of HPc on Cu(111) ($U = -500$ mV). The linear fit with a slope of $m = 1.062 \pm 0.043$ confirms that the tautomerization is a one-electron process. (b) Injection-energy-dependent HPc tautomerization yield on Cu(111) and Ag(111). The data are fitted with multiple energy thresholds. Literature values of the N-H stretching mode taken from Refs. [27,28] are indicated by vertical lines at ± 408 and ± 816 meV.

and detected by a sudden change of the relative tip height. This is evidenced by the temporal trace of the recorded tip height in Fig. 1(d) which clearly shows four distinct levels that correspond to the different tautomers.

An analysis of the current- and voltage-dependent switching rate provides a detailed understanding of the tautomerization process. For HPc on Ag(111) it has been shown that tautomerization processes are induced by single charge carriers [26]. To verify this for HPc on Cu(111), we determined the tunneling-current-dependent tautomerization rate in the range between $350 \text{ pA} \leq I \leq 4.05 \text{ nA}$ at a bias voltage $U = -500$ mV. The resulting data are plotted in a double-logarithmic representation in Fig. 2(a). By fitting the data, we obtain a slope of about 1, thereby confirming a linear dependency between the switching rate and the tunneling current. This result corroborates that the tautomerization of HPc on Cu(111) is indeed triggered by a one-electron process, as previously demonstrated for HPc on Ag(111) [26]. The one-to-one correspondence between the amount of injected

TABLE I. Threshold energies for tautomerization of HPc on Cu(111) extracted from fits compared to the energy of the N-H stretching mode in HPc.

	$E_{\text{th},1}$ (meV)	$E_{\text{th},2}$ (meV)
Positive voltage	399 ± 57	803 ± 76
Negative voltage	424 ± 40	814 ± 11
N-H stretching mode [27,28]	408	816

charge carriers and the tautomerization rate allows us to tune the tunneling current such that we achieve an optimal tautomerization rate at various charge carrier energies for the following measurements.

For further analysis, we therefore calculated the tautomerization yield per μC by normalizing the number of observed tautomerization events to the number of injected charge carriers obtained by multiplying the injection current with the injection time. To analyze the energy dependence of the tautomerization process, we determined the electron yield for HPc tautomerization for a wide range of bias voltages. The results for Cu(111) (blue dots) are presented in Fig. 2(b) and compared to Ag(111) (red). Overall, we find that the electron yield for HPc on Cu(111) is about one order of magnitude lower than on Ag(111). This clearly exceeds any potential influence from different STM tips [29]. For both substrates the electron yield monotonically increases with the absolute value of the injection energy $|E - E_F|$. This increase is not continuous but particularly steep at some injection energies and much lower at others. As indicated by vertical black lines, the transition between slowly and steeply increasing electron yields occurs symmetrically around the Fermi energy at about ± 400 and ± 800 meV and seems to be independent of the particular substrate. The threshold energies for HPc on Cu(111) are determined from fits [31] and presented in Table I. It has been shown for HPc and H_2Pc on Ag(111) that these energies correspond to the N-H stretching mode [16]. This strongly suggests that the tautomerization process is induced by the inelastic excitation of vibrational modes, although other mechanisms like resonant tunneling cannot strictly be excluded [30].

For Ag(111), a third increase at ± 160 meV has previously been attributed to an in-plane bound mode [16]. Due to the low switching rate below 400 meV, this steplike increase cannot be confirmed on Cu(111). The insufficient switching rate might be caused by a higher energy barrier between the tautomeric states, potentially caused by a stronger bond between the molecule and the Cu(111) surface as compared to Ag(111). This assumption is supported by the generally lower tautomerization rate and the stronger increases at around ± 400 and ± 800 meV. The difference of one order of magnitude for the low-energy increase (≈ 400 meV) can be clearly seen in Fig. 2(b). For the high-energy increase (≈ 800 meV), the quotients $q^{+(-)} = \frac{\eta_{1000}}{\eta_{700}}$ are given in Table II, where η is the electron yield at the given energies for positive (negative) voltages. The factor $q_{\text{Cu}}^{+(-)}/q_{\text{Ag}}^{+(-)} \approx 2$ (1.5) corroborates the assumption of a higher tautomerization barrier for HPc on Cu(111) as compared to HPc on Ag(111).

TABLE II. Quotients $q^{+(-)} = \frac{\eta_{1000}}{\eta_{700}}$ of the tautomerization rates at $\pm(-)1000$ meV and $\pm(-)700$ meV for HPc on Cu(111) and Ag(111).

	q^+	q^-
Cu(111)	7.94 ± 0.24	3.89 ± 0.16
Ag(111)	3.99 ± 0.07	2.79 ± 0.18

B. Molecular nanoprobe

HPc on Cu(111) exhibits a reversible, charge-carrier-induced tautomerization and therefore fulfills all requirements for a novel technique which is capable of detecting ballistic charge carrier transport on length scales of a few nanometers, termed MOlecular NANoprobe (MONA) [21]. In MONA, charge carriers are injected at a distance d from the molecule; see Fig. 3(a). Some of the injected charge carriers propagate toward the molecule, where they may inelastically scatter and induce a tautomerization. As described above in Fig. 1(c), this change of the tautomeric state can be detected in STM images. Therefore, an analysis of the switching probability provides access to the substrate's transport properties between the charge carrier injection point, i.e., the location of the tip apex, and the molecule, which acts as a charge detector.

To guarantee the reliability of MONA, a number of conditions have to be fulfilled. First, noninvasive STM imaging parameters must exist. For HPc on Cu(111) or Ag(111), for example, this condition is fulfilled at $U = 50$ mV and $I = 50$ pA; see Fig. 2(b). At these imaging parameters the state of the molecule after each pulse n can be probed and compared with the state before the pulse, $n - 1$, thereby allowing for the identification of switching events. Second, to reduce the probability of multiple tautomerization events during a single excitation pulse to an insignificant level, the pulse length has to be adjusted to a tautomerization probability between 5% and 15% per pulse. The electron yield η is calculated by the number of observed tautomerization events N_T divided by the total amount of injected charge Q . Third, to achieve a low error bar, given by $\Delta\eta = \sqrt{\eta(1-\eta)/Q}$, all data points presented in this study are given as the average over at least 1000 excitation pulses. Only if these three conditions are fulfilled, the resulting electron yield contains valuable information about the transport properties on the nanometer scale.

To examine whether the charge carrier transport on Cu(111) exhibits potential anisotropies, the STM tip was positioned at various injection points on a circle with a radius $d = 4$ nm around the detector molecule; see green stars in Fig. 3(a). The angle α between two adjacent injection points in the lower right quadrant which spans between $\alpha = 0^\circ$ (along closed-packed $[01\bar{1}]$ axis) and $\alpha = 90^\circ$ ($[2\bar{1}\bar{1}]$), amounts to 15° . Furthermore, we performed measurements at two reference points at $\alpha = 180^\circ$ and 270° . All data were taken at a constant injection energy $E = 900$ meV.

The measured electron yield is plotted in a polar coordinate system in Fig. 3(b). The inset shows the schematic structure of the molecule and the underlying Cu(111) surface. First, we would like to emphasize that the twofold symmetry of the surface-molecule system manifests in the 20% difference in electron yield measured between 0° and 90° . The reference

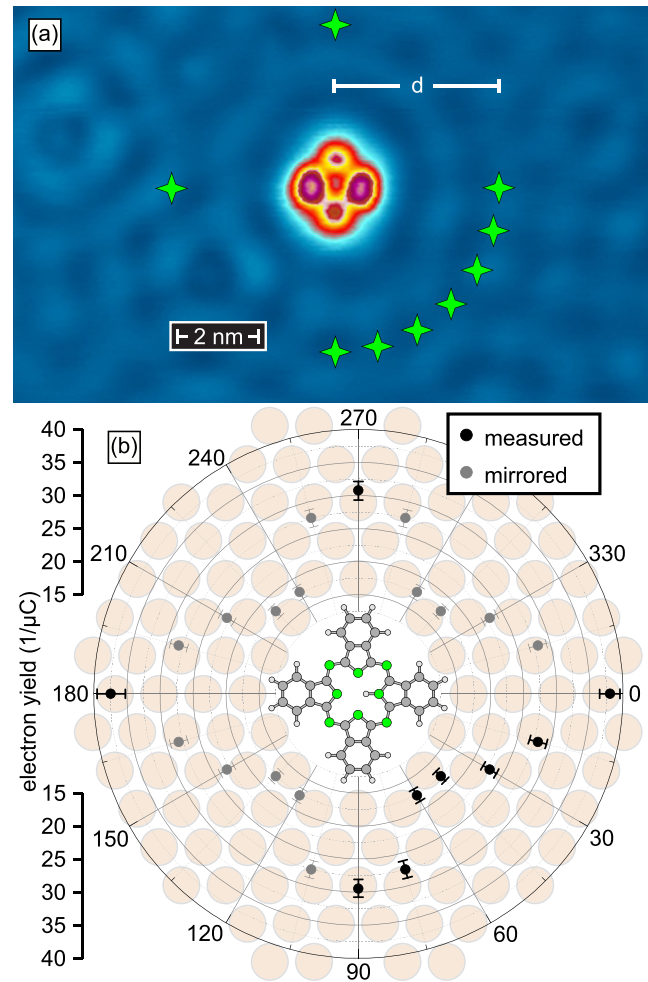


FIG. 3. (a) STM topography image ($U = 50$ mV, $I = 50$ pA) of a HPc molecule on Cu(111). The injection points are marked as green stars in a distance d from the molecular center. (b) MONA electron yield (injection energy $E = 900$ meV) of the HPc detector molecule. A 20% difference is measured between $\alpha = 0^\circ$ and $\alpha = 90^\circ$, caused by the twofold symmetry of the surface-molecule system. To better visualize the symmetries, measured (black) data points are mirrored (gray) along the $[01\bar{1}]$ and $[2\bar{1}\bar{1}]$ axes and superimposed with the schematic structure of the molecule and surface.

points at 180° and 270° match their counterparts and confirm this twofold symmetry. Furthermore, when changing the injection point from 0° to 45° , the electron yield continuously decreases by about a factor of 2, and then increases from 60° to 90° by about a factor of 1.5. Since the Cu(111) surface layer exhibits a sixfold symmetry, the observed twofold symmetry cannot originate from transport-related properties. Instead, the anisotropy must be caused by an inhomogeneous coupling of the molecule to the surface.

The results presented in Fig. 3(b) have some implications on how measurements need to be performed, for example when in the next step the energy dependence of charge carrier transport on Cu(111) is determined by changing the injection energy during excitation pulse. Since the inhomogeneous coupling between the molecule and the surface implies a significant angle-dependent anisotropy, the STM tip has to

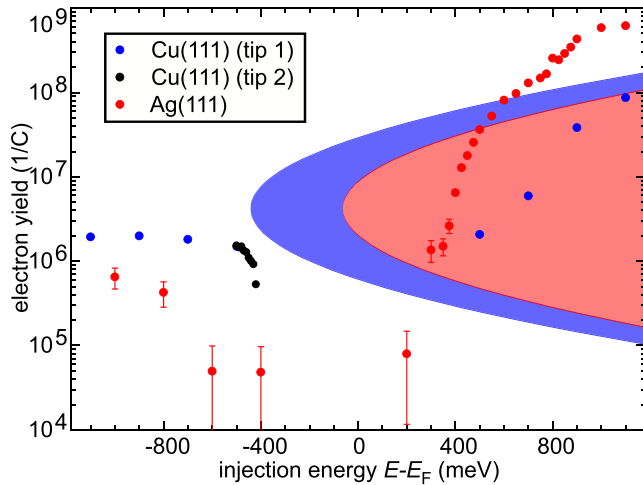


FIG. 4. Injection-energy-dependent tautomerization rates of HPC on Cu(111) (blue and black data points indicating different STM tips) and Ag(111) (red) measured with MONA at a tip-sample distance $d = 4$ nm along the closed-packed $[01\bar{1}]$ axis $[0^\circ]$ in Fig. 3(b)]. Two colored parabolas illustrate the energy range where the Cu(111) and the Ag(111) surface states exist. Their onset energies amount to $E_{\text{on}}^{\text{Cu}} = -450$ meV and $E_{\text{on}}^{\text{Ag}} = -63$ meV, respectively.

be positioned at a fixed injection point such that not only the tip-molecule distance d but also the angle α remain constant. To better exemplify the investigated transport properties, the results obtained on Cu(111) will be compared to data measured under identical conditions on Ag(111).

As illustrated by two colored parabolas in the background of Fig. 4, both surfaces exhibit a surface state with comparable effective electron masses $m_{\text{eff}}^{\text{Cu}} = 0.41m_e$ and $m_{\text{eff}}^{\text{Ag}} = 0.38m_e$ [32], but very different onset energies of $E_{\text{on}}^{\text{Cu}} = -450$ meV and $E_{\text{on}}^{\text{Ag}} = -63$ meV [33]. Keeping in mind that the tautomerization of HPC on either of these two surfaces requires a threshold energy $E_{\text{th}} = 408$ meV, one realizes that charge carrier transport via the Ag(111) surface state can only occur at positive bias voltages. In contrast, the lower onset energy of the Cu(111) surface state also allows for the injection of high-energy holes (originating from an electron that tunnels out of the surface state into the tip). Even though bulk bands also exist on both surfaces, due to geometric reasons charge carriers in bulk states are expected to possess a significantly lower probability to reach the molecule and therefore result in a much lower electron yield with the MONA technique.

Indeed, these expectations are confirmed by the experimental data presented in Fig. 4. It shows the electron yield measured on Cu(111) (black and blue data points) in comparison to Ag(111) (red). For both substrates, a monotonic increase by at least two orders of magnitude is observed at positive energies. On Ag(111) we recognize two energy ranges where the electron yield rises particularly strongly with increasing injection energy. These energy ranges agree well with the excitation barriers $E_{\text{th},1} = 408$ meV and $E_{\text{th},2} = 816$ meV related to the N-H stretching mode of the HPC molecule [27,28]. On Cu(111) these excitation barriers cannot be identified due to the insufficient energy resolution. In

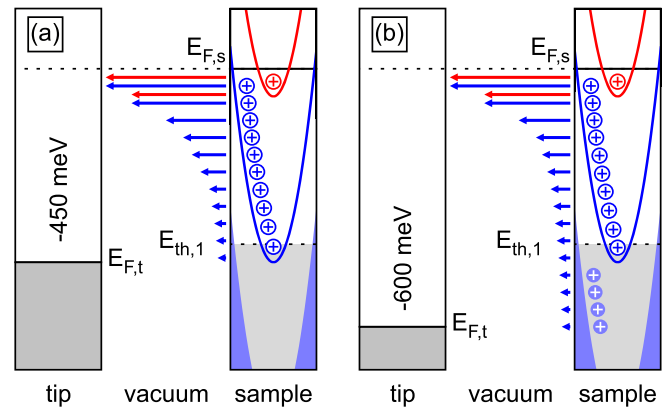


FIG. 5. Scheme of the tunneling process for bias voltages of (a) $U = -450$ mV and (b) $U = -600$ mV. The surface state of Cu(111) is represented by an upward opened blue parabola; the bulk states are given by the blue shaded area. The length of the arrows symbolizes the amount of tunneling electrons at the given energy. The resulting holes are shaded for bulk states and nonshaded for surface states. States below the threshold energy $E_{\text{th},1} = -408$ meV are highlighted in gray. For comparison the surface state of Ag(111) is shown in red.

agreement with the observations made for on-top measurements, cf. Fig. 2(b), the electron yield for Cu(111) is roughly one order of magnitude lower than for Ag(111).

At negative bias voltages, where electrons tunnel from occupied sample states into empty tip states and thereby create a hole in the metal's conduction band, the behavior observed on Ag(111) and Cu(111) is strikingly different. On Ag(111) the surface state onset is at $E_{\text{on}}^{\text{Ag}} = -63$ meV, which is below the energy threshold for tautomerization of HPC. Therefore, at injection energies $E \geq E_{\text{th},1}$, only holes in bulk states can potentially induce a tautomerization. For these, as mentioned earlier, a very low electron yield is expected, which is consistent with the results presented in Fig. 4.

In contrast, the Cu(111) surface state onset is energetically located at around $E_{\text{on}}^{\text{Cu}} = -450$ meV, i.e., at an energy slightly above $E_{\text{th},1}$, where tautomerization events may already be triggered. Indeed, the data of Fig. 4 reveal a steep increase of the electron yield right at $E - E_F \approx -400$ meV. Below the surface state onset, i.e., at $E - E_F < -450$ meV, however, no further increase but a flat plateau with an almost constant electron yield is observed, in stark contrast to the steep increase of the electron yield detected at positive bias.

IV. DISCUSSION

The data presented in Fig. 4 can qualitatively be explained by considering a schematic potential diagram of tunneling processes at negative sample bias values U . Figure 5(a) shows the situation for $U = -450$ meV, where the tip's Fermi level is just aligned with the bottom of the Cu(111) surface state at $E_{\text{on}}^{\text{Cu}}$. As symbolized by red arrows, tunneling processes of electrons from the Ag(111) surface state into empty states of the tip produce holes in the parabolically dispersing surface

state band, but are limited to the narrow energy range between the Fermi level and $E_{\text{on}}^{\text{Ag}} = -63$ meV. Since $E_{\text{on}}^{\text{Ag}} \ll E_{\text{th},1}$, relaxation of the excited hole in the Ag(111) surface state band with electrons cannot release the energy required to trigger HPC tautomerization.

The situation is significantly different for tunneling processes that occur between occupied states in the Cu(111) surface state (blue) and the tip, since $E_{\text{on}}^{\text{Cu}} \gtrsim E_{\text{th},1}$. Although the majority of holes produced within the surface state band, namely those in the energy range between $E_{\text{F}}^{\text{Cu}} > E > E_{\text{th},1}$, still possess an energy insufficient to trigger HPC tautomerization, there exists a small energy window with holes between $E_{\text{th},1} > E > E_{\text{on}}^{\text{Cu}}$ where the relaxation of electrons from $E \approx E_{\text{F}}^{\text{Cu}}$ may produce an energy $E > E_{\text{th},1}$. The transfer of energy from these relaxation processes into the molecule leads to the rapid increase of electron yield observed in this energy window in Fig. 4.

This is in clear contrast to the unoccupied states, where the surface states of Cu(111) and Ag(111) disperse within the gap of the projected bulk band structure well above the Fermi level [34], as illustrated in the potential diagram for $eU = -600$ meV in Fig. 5(b). In the energy range between $E_{\text{on}}^{\text{Cu}} = -450$ and -600 meV, holes can only be created in bulk bands, where they have a much lower probability of reaching the detector molecule and trigger tautomerization events. Therefore, bulk states have an insignificant contribution to the overall transport, resulting in an essentially constant tautomerization electron yield observed in this energy range in Fig. 4.

V. CONCLUSION

In this study we characterized the tautomerization process of HPC on Cu(111). The tautomerization rate is symmetric around the Fermi level and exhibits two energy thresholds at around -400 and -800 meV. Similarly to HPC on Ag(111), a single charge carrier of sufficient energy can excite a N-H stretching mode that in turn can induce a tautomerization. These tautomerization events can be used in the MONA technique for the detection of charge carrier transport. Our MONA measurements provide evidence for an inhomogeneous coupling of HPC to the Cu(111) substrate, in agreement with the symmetry mismatch between the sixfold-symmetric substrate and fourfold-symmetric molecule. A detailed comparison of the transport properties of the Ag(111) and the Cu(111) surface corroborates that the MONA technique can be utilized to detect both electron and hole transport and is sensitive to the band structure.

ACKNOWLEDGMENTS

This work was supported by the DFG through SFB 1170 (project A02). We also acknowledge financial support by the Deutsche Forschungsgemeinschaft (DFG; German Research Foundation) under Germany's Excellence Strategy through Würzburg-Dresden Cluster of Excellence on Complexity and Topology in Quantum Matter, *ct.qmat* (EXC 2147; Project ID 390858490). The publication was supported by the Open Access Publication Fund of the University of Würzburg.

APPENDIX: DISTINCTION OF TAUTOMERIC STATES

The correct determination of the tautomeric state of HPC on Cu(111) is essential for this study. While the tautomers 1 and 4 in Fig. 1(c) of the main text can easily be assigned due to the elevation of the corresponding arm along the $[2\bar{1}\bar{1}]$ axis, the distinction between tautomers 2 and 3 is difficult [see Fig. 6(a)]. To highlight the slight elongation of the corresponding arms line profiles along the $[01\bar{1}]$ axis are shown in Fig. 6(b). While the maxima of the arms are at a similar position for both tautomers, the minimum between the arms shifts by approximately 0.1 nm. This shift can also be seen in Fig. 6(c), where scans of both tautomers are overlapped.

For the analysis of MONA measurements, both a line profile and an overlap would be much too time consuming. For the purpose of determining the switching rate, however, it is not necessary to analyze the exact state of each scan. Instead, it is sufficient to identify any change in the tautomeric state between two successive scans, which is possible with the naked eye (see the movie in the Supplemental Material [35]).

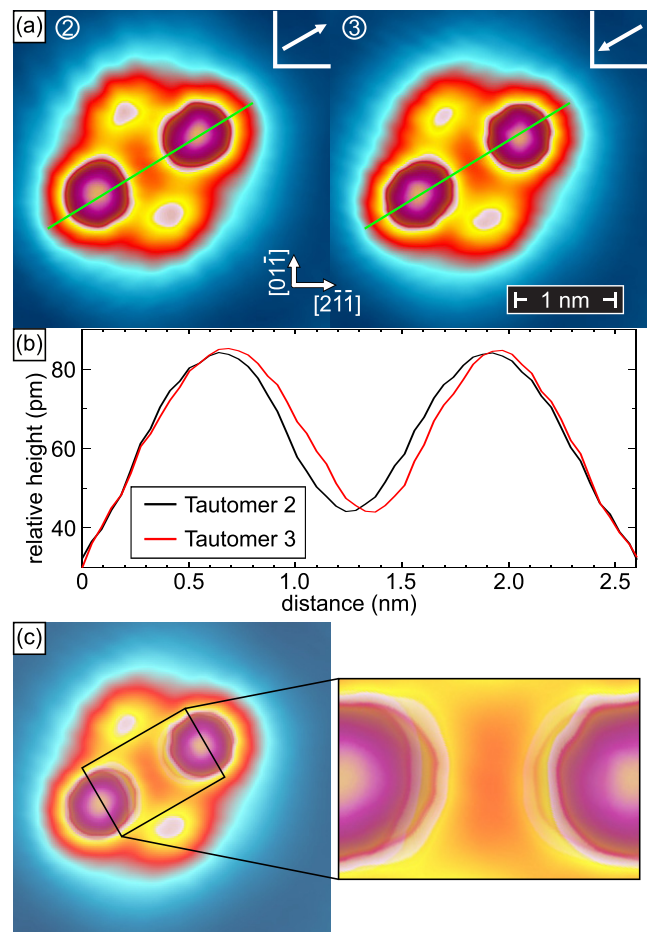


FIG. 6. (a) Topographic scans of tautomers 2 and 3 ($U = 50$ mV, $I = 50$ pA). White arrows indicate the binding position of the central hydrogen. For better distinction line profiles along the green lines (black for 2, red for 3) are shown in (b). The elongation of arms along the $[01\bar{1}]$ axis can be seen in the overlap of tautomers in (c). The relevant center of the molecule is enlarged.

- [1] M. Walzl, Reliability of miniaturized transistors from the perspective of single-defects, *Micromachines* **11**, 736 (2020).
- [2] T. Zhou and D. Gall, Resistivity scaling due to electron surface scattering in thin metal layers, *Phys. Rev. B* **97**, 165406 (2018).
- [3] F. Giannazzo, S. Sonde, R. L. Nigro, E. Rimini, and V. Raineri, Mapping the density of scattering centers limiting the electron mean free path in graphene, *Nano Lett.* **11**, 4612 (2011).
- [4] J. J. Plombon, E. Andideh, V. M. Dubin, and J. Maiz, Influence of phonon, geometry, impurity, and grain size on copper line resistivity, *Appl. Phys. Lett.* **89**, 113124 (2006).
- [5] Q. Huang, C. M. Lilley, and M. Bode, Surface scattering effect on the electrical resistivity of single crystalline silver nanowires self-assembled on vicinal Si(001), *Appl. Phys. Lett.* **95**, 103112 (2009).
- [6] S. Dutta, K. Sankaran, K. Moors, G. Pourtois, S. Van Elshocht, J. Bömmels, W. Vandervorst, Z. Tókei, and C. Adelman, Thickness dependence of the resistivity of platinum-group metal thin films, *J. Appl. Phys.* **122**, 025107 (2017).
- [7] P. Y. Zheng, T. Zhou, B. J. Engler, J. S. Chawla, R. Hull, and D. Gall, Surface roughness dependence of the electrical resistivity of W(001) layers, *J. Appl. Phys.* **122**, 095304 (2017).
- [8] P. Zheng and D. Gall, The anisotropic size effect of the electrical resistivity of metal thin films: Tungsten, *J. Appl. Phys.* **122**, 135301 (2017).
- [9] N. A. Lanzillo, H. Dixit, E. Milosevic, C. Niu, A. V. Carr, P. Oldiges, M. V. Raymond, J. Cho, T. E. Standaert, and V. K. Kamineni, Defect and grain boundary scattering in tungsten: A combined theoretical and experimental study, *J. Appl. Phys.* **123**, 154303 (2018).
- [10] T. Zhou, P. Zheng, S. C. Pandey, R. Sundararaman, and D. Gall, The electrical resistivity of rough thin films: A model based on electron reflection at discrete step edges, *J. Appl. Phys.* **123**, 155107 (2018).
- [11] F. Wenner, A method of measuring earth resistivity, *Bulletin of the Bureau of Standards* **12**, 469 (1915).
- [12] I. Miccoli, F. Edler, H. Pfnür, and C. Tegenkamp, The 100th anniversary of the four-point probe technique: The role of probe geometries in isotropic and anisotropic systems, *J. Phys.: Condens. Matter* **27**, 223201 (2015).
- [13] J. Yang, D. Sordes, M. Kolmer, D. Martrou, and C. Joachim, Imaging, single atom contact and single atom manipulations at low temperature using the new ScientaOmicron LT-UHV-4 STM, *Eur. Phys. J. Appl. Phys.* **73**, 10702 (2016).
- [14] M. Kolmer, P. Brandimarte, J. Lis, R. Zuzak, S. Godlewski, H. Kawai, A. Garcia-Lekue, N. Lorente, T. Frederiksen, C. Joachim, D. Sanchez-Portal, and M. Szymonski, Electronic transport in planar atomic-scale structures measured by two-probe scanning tunneling spectroscopy, *Nat. Commun.* **10**, 1573 (2019).
- [15] P. Liljeroth, J. Repp, and G. Meyer, Current-induced hydrogen tautomerization and conductance switching of naphthalocyanine molecules, *Science* **317**, 1203 (2007).
- [16] J. Kügel, L. Klein, M. Leisegang, and M. Bode, Analyzing and tuning the energetic landscape of H₂Pc tautomerization, *J. Phys. Chem. C* **121**, 28204 (2017).
- [17] Y. Sainoo, Y. Kim, T. Okawa, T. Komeda, H. Shigekawa, and M. Kawai, Excitation of Molecular Vibrational Modes with Inelastic Scanning Tunneling Microscopy Processes: Examination through Action Spectra of *cis*-2-Butene on Pd(110), *Phys. Rev. Lett.* **95**, 246102 (2005).
- [18] M. Leisegang, R. Schindhelm, J. Kügel, and M. Bode, Anisotropic Ballistic Transport Revealed by Molecular Nanoprobe Experiments, *Phys. Rev. Lett.* **126**, 146601 (2021).
- [19] J. N. Ladenthin, L. Grill, S. Gawinkowski, S. Liu, J. Waluk, and T. Kumagai, Hot carrier-induced tautomerization within a single porphycene molecule on Cu (111), *ACS Nano* **9**, 7287 (2015).
- [20] J. Kügel, M. Leisegang, M. Böhme, A. Krönlein, A. Sixta, and M. Bode, Remote single-molecule switching: Identification and nanoengineering of hot electron-induced tautomerization, *Nano Lett.* **17**, 5106 (2017).
- [21] M. Leisegang, J. Kügel, L. Klein, and M. Bode, Analyzing the wave nature of hot electrons with a molecular nanoprobe, *Nano Lett.* **18**, 2165 (2018).
- [22] M. Leisegang, M. Bode, and J. Kügel, Analyzing the influence of substituents on proton tautomerization—comparison of tetra-*tert*-butyl phthalocyanine isomers, *J. Phys. Chem. C* **122**, 29633 (2018).
- [23] F. Reinert, G. Nicolay, S. Schmidt, D. Ehm, and S. Hüfner, Direct measurements of the *L*-gap surface states on the (111) face of noble metals by photoelectron spectroscopy, *Phys. Rev. B* **63**, 115415 (2001).
- [24] L. Bartels, G. Meyer, and K.-H. Rieder, Basic Steps of Lateral Manipulation of Single Atoms and Diatomic Clusters with a Scanning Tunneling Microscope Tip, *Phys. Rev. Lett.* **79**, 697 (1997).
- [25] W. Auswärter, S. Seufert, F. Bischoff, D. Eciija, S. Vijayaraghavan, S. Joshi, F. Klappenberger, N. Samudrala, and J. B. Barth, A surface-anchored molecular four-level conductance switch based on single proton transfer, *Nat. Nanotechnol.* **7**, 41 (2012).
- [26] J. Kügel, A. Sixta, M. Böhme, A. Krönlein, and M. Bode, Breaking degeneracy of tautomerization—metastability from days to seconds, *ACS Nano* **10**, 11058 (2016).
- [27] X. Zhang, Y. Zhang, and J. Jiang, Isotope effect in the infrared spectra of free-base phthalocyanine and its *N,N*-dideuterio-derivative: Density functional calculations, *Vib. Spectrosc.* **33**, 153 (2003).
- [28] C. Murray, N. Dozova, J. G. McCaffrey, S. FitzGerald, N. Shafizadeh, and C. Crepin, Infra-red and Raman spectroscopy of free-base and zinc phthalocyanines isolated in matrices, *Phys. Chem. Chem. Phys.* **12**, 10406 (2010).
- [29] J. Kügel, T. Zenger, M. Leisegang, and M. Bode, On the impact of geometrical factors on hot electron-induced tautomerization, *J. Phys. Chem. C* **123**, 17056 (2019).
- [30] R. Harsh, F. Joucken, C. Chacon, V. Repain, Y. Girard, A. Bellec, S. Rousset, R. Sporcken, A. Smogunov, Y. Dappe, and J. Lagoute, Controlling hydrogen-transfer rate in molecules on graphene by tunable molecular orbital levels, *J. Phys. Chem. Lett.* **10**, 6897 (2019).
- [31] K. Motobayashi, Y. Kim, H. Ueba, and M. Kawai, Insight Into Action Spectroscopy for Single Molecule Motion and Reactions through Inelastic Electron Tunneling, *Phys. Rev. Lett.* **105**, 076101 (2010).
- [32] A. Tamai, W. Meevasana, P. D. C. King, C. W. Nicholson, A. de la Torre, E. Rozbicki, and F. Baumberger, Spin-orbit splitting of

- the Shockley surface state on Cu(111), *Phys. Rev. B* **87**, 075113 (2013).
- [33] K. Yaji, A. Harasawa, K. Kuroda, R. Li, B. Yan, F. Komori, and S. Shin, Rashba spin splitting of L -gap surface states on Ag(111) and Cu(111), *Phys. Rev. B* **98**, 041404(R) (2018).
- [34] A. Goldmann, V. Dose, and G. Borstel, Empty electronic states at the (100), (110), and (111) surfaces of nickel, copper, and silver, *Phys. Rev. B* **32**, 1971 (1985).
- [35] See Supplemental Material at <http://link.aps.org/supplemental/10.1103/PhysRevResearch.4.043016> for a short movie of consecutive MONA scans.